THE JOURNAL OF PHYSICAL CHEMISTRY C
A JOURNAL OF THE AMERICAN CHEMICAL SOCIETY

pubs.acs.org/JPCC
Article

On the Electronic, Mechanical and Optical Properties of Superhard Cross-Linked Carbon Nanotubes (Tubulanes)

Raphael M. Tromer, Bruno Ipaves, Marcelo L. Pereira Junior,* Cristiano F. Woellner, Kun Cai, and Douglas S. Galvao*

Cite This: J. Phys. Chem. C 2026, 130, 3624−3631

ABSTRACT: We have investigated the electronic, optical, and mechanical properties of six structures belonging to the Tubulanes-cross-linked carbon nanotube family, using Density Functional Theory (DFT) with the Generalized Gradient Approximation (GGA) and the Perdew−Burke−Ernzerhof (PBE) functional. Our results highlight the remarkable anisotropic mechanical behavior of these materials, distinguishing them from isotropic structures, such as diamond. Notably, the 8-tetra-22 structure has a higher Young's modulus (Y_M) along the *z*-direction compared to diamond. Unlike diamonds, the mechanical properties of Tubulanes are direction-dependent, exhibiting significant variations in Young's Modulus (2.3 times). Additionally, the Poisson's ratio is highly anisotropic, with at least one direction exhibiting a value close to zero. The inherent anisotropy of these materials enables tunable mechanical properties that depend on the direction of applied stress. Regarding their electronic properties, all Tubulane structures studied possess indirect electronic band gaps, dominated by 2p orbitals. The band dispersion is relatively high, with band gaps ranging from 0.46 to 2.74 eV, all of which are smaller than that of diamond. Notably, the 16-tetra-22 structure exhibits the smallest bandgap (0.46 eV), making it particularly interesting for electronic applications. Additionally, these structures exhibit porosity, which offers advantages over denser materials, such as diamond. Given recent advances in the synthesis of 3D carbon-based materials, the synthesis of tubulane-like structures is within current technological capabilities.

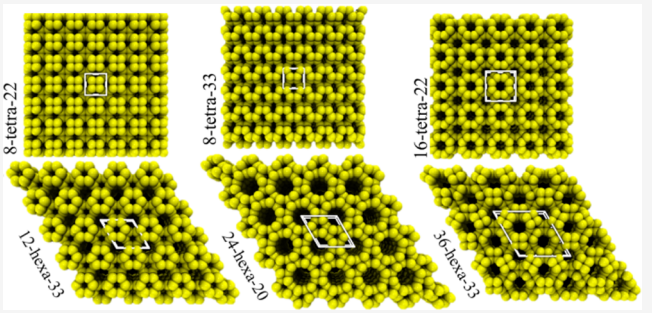

INTRODUCTION

The search for materials with exceptional mechanical, electronic, and optical properties has generated significant interest in carbon-based nanostructures, such as carbon nanotubes (CNTs) and graphene. Among these, the cross-linked carbon nanotube structures, known as tubulanes, represent a class of materials with remarkable strength, stability, and electronic properties. Notably, tubulanes exhibit super hardness and structural integrity under extreme conditions, making them attractive candidates for a wide range of applications, from impact-resistant materials to next-generation electronics.[1,2]

Several studies have demonstrated that specific arrangements of CNTs can significantly impact the mechanical and electronic properties of the resulting structure. For example, high-pressure CNT networks exhibit enhanced mechanical strength and resilience due to the interlinked nature of the tubes.[1−3] The electronic properties of tubulanes, like those of other carbon nanomaterials, are highly dependent on their atomic configuration. Similar to other carbon allotropes, tubulanes can exhibit either metallic or semiconducting behavior depending on their topology.[3−6] Although the experimental synthesis of Tubulanes has not yet been fully achieved, several studies suggest that such cross-linked carbon nanotube networks could be obtained through high-pressure compression or related polymerization processes of carbon nanotube bundles.[1−3]

Theoretical studies have played a crucial role in predicting the behavior of these complex nanostructures. Density functional theory (DFT) has proven to be a reliable method for investigating various properties, including the electronic and optical characteristics of carbon-based materials, offering valuable insights into their electronic band gaps.[2,7,8] Recent DFT and multiscale studies provide a more comprehensive context for the exploration of the electronic, optical, and structural properties of complex nanomaterials,[9−11] providing a relevant framework for the investigation of Tubulanes in the present work. In addition, molecular dynamics simulations are frequently employed to explore thermal stability and mechanical responses under varying conditions.[1−3] The combination of these simulation techniques has significantly improved our

Received: December 22, 2025
Revised: February 10, 2026
Accepted: February 11, 2026
Published: February 19, 2026

https://doi.org/10.1021/acs.jpcc.5c08652
J. Phys. Chem. C 2026, 130, 3624−3631

ability to predict and tailor the properties of tubulanes and other nanostructures.[2]

A promising aspect of tubulanes is their potential for novel applications in diverse fields. The combination of mechanical strength and electronic versatility in these diamond-like superhard phases could play a key role in areas such as energy storage, sensing, and UV collectors.[2,7,12] Recent studies have also highlighted their potential use in ballistic applications.[3] These emerging applications underline the need for further investigation into their optical properties and structural stability under diverse environmental conditions.

In this work, we have investigated the structural, mechanical, electronic, and optical properties of tubulanes using DFT and ab initio molecular dynamics (AIMD) simulations. Building upon prior theoretical studies, we have examined the stability of two families of tubulanes: the tetragonal and hexagonal families. The tetragonal structures, named 8-tetra-22, 8-tetra-33, and 16-tetra-22, and the hexagonal structures, named 12-hexa-33, 24-hexa-20, and 36-hexa-33, were comprehensively analyzed. The six selected structures, comprising three tetragonal and three hexagonal models, were chosen as representative examples of distinct topologies within the Tubulane family, allowing for a systematic comparison of their structure−property relationships. We assess their mechanical behavior under uniaxial compression and investigate their electronic and optical properties, providing new insights into their potential for ultraviolet-blocking applications.

METHODOLOGY

We have carried out DFT simulations using the CASTEP[13] and SIESTA[14] codes. CASTEP is a plane-wave basis-set method. We have used CASTEP for the mechanical and electronic analyses of the tubulanes. The calculations were performed using the generalized gradient approximation (GGA) and the Perdew−Burke−Ernzerhof (PBE)[15] functional to represent the exchange−correlation term. To improve the description of noncovalent interactions in the GGA-PBE calculations, we used a semiempirical dispersion correction scheme of Tkatchenko and Scheffler (PBE + D).[16] To replace the core electrons in each atomic species, we adopted norm-conserving pseudopotentials.[17] We used the Monkhorst−Pack scheme to represent the k-points of integration in the Brillouin zone, with k-points set to $5 \times 5 \times 10$ and an energy cutoff of 300 eV.[18]

The optimization process was carried out using the Broyden, Fletcher, Goldfarb, and Shanno (BFGS) scheme.[19] Both atoms and lattice parameters were optimized simultaneously. We considered the forces in each atom to be equal to 0.01 eV/Å as the convergence criterion. We adopted an energy variation of less than 0.5×10^{-6} eV/atom for each self-consistent field (SCF) cycle as the convergence criterion. The elastic properties were extracted using the geometrically optimized structures. The bulk modulus (B), Young's modulus (Y_M), and Poisson's ratios (ν) were obtained from the 6×6 elastic constant tensor calculated using the CASTEP Elastic Constants module. These parameters were derived using standard tensor relations within the Voigt−Reuss−Hill averaging scheme, as implemented in CASTEP. We have also investigated the structural stability of the tubulane structures at room temperature by carrying ab initio molecular dynamics (AIMD) simulations using an NPT ensemble, with a time step of 1 fs. The unit cell was replicated 2 times along each direction.

For optical property simulations, we used the SIESTA software,[14] a DFT-based code that employs localized atomic orbital basis sets. We have used the functional GGA/PBE, which is equivalent to that used in CASTEP simulations. We have used the same geometries obtained with the CASTEP and verified that SIESTA and CASTEP produce practically identical electronic bandgap values.

We used the Troullier−Martins pseudopotentials in the SIESTA simulations to describe core electrons with a basis set double-ζ plus polarization functions (DZP). The cutoff value for kinetic energy is 300 Ry, and the k-points are $12 \times 12 \times 12$, using the Monkhorst−Pack scheme.

The optical simulations were modeled by a system immersed in the region of the externally applied electrical field, operating in the linear regime associated with electromagnetic radiation. In the linear regime, the typical value of the external electrical field, which does not cause significant distortion in the structures, is 1.0 V/Å.[20] We have considered polarization along a single direction (x, y, or z) separately.

The starting point consists of obtaining the real part ϵ_1 and imaginary part ϵ_2 of the dielectric constant function. These quantities are extracted directly from the Kramers−Kronig relation and Fermi's golden rule, respectively.

All optical coefficients are calculated by relating the real and imaginary parts of the dielectric constant function. The absorption coefficient α, the reflectivity R, and the refractive index η are given by

$$\alpha(\omega) = \sqrt{2}\,\omega[(\epsilon_1^2(\omega) + \epsilon_2^2(\omega))^{1/2} - \epsilon_1(\omega)]^{1/2} \quad (1)$$

$$R(\omega) = \left[\frac{(\epsilon_1(\omega) + i\epsilon_2(\omega))^{1/2} - 1}{(\epsilon_1(\omega) + i\epsilon_2(\omega))^{1/2} + 1}\right]^2, \text{and} \quad (2)$$

$$\eta(\omega) = \frac{1}{\sqrt{2}}[(\epsilon_1^2(\omega) + \epsilon_2^2(\omega))^{1/2} + \epsilon_1(\omega)]^2 \quad (3)$$

The accuracy of the optical coefficients is related to a good description of the electronic bandgap value. In other words, the more accurate the bandgap value is, the more precisely the optical transitions will be described. It is well-known that GGA/PBE does not accurately reproduce the electronic band gap values of semiconductor materials. This approximation tends to underestimate the experimental value obtained with more robust methods.[21] Other approximations, such as the HSE06 hybrid functional, yield more accurate bandgap values.[22] Here, we used the HSE06 functional implemented in the Gaussian16 software to obtain the electronic bandgap energy of carbon tubulanes with higher precision. We used parameters that yield a good description of the bandgap in cubic diamond as a reference.

Then, we use the scissor operator available in SIESTA to correct the optical transitions using the electronic band gap values extracted from Gaussian16. In SIESTA, this correction is defined by a quantity called the scissor operator, which produces a shift in the unoccupied states, given by

$$\text{scissor} = E_{\text{gap}}^{\text{HSE06}} - E_{\text{gap}}^{\text{PBE}} \quad (4)$$

In the literature, some works have employed this approximation to correct the optical transitions generated with the scissor operator, yielding results similar to those of more sophisticated methods, such as GW ones.[23,24]

https://doi.org/10.1021/acs.jpcc.5c08652
J. Phys. Chem. C 2026, 130, 3624−3631

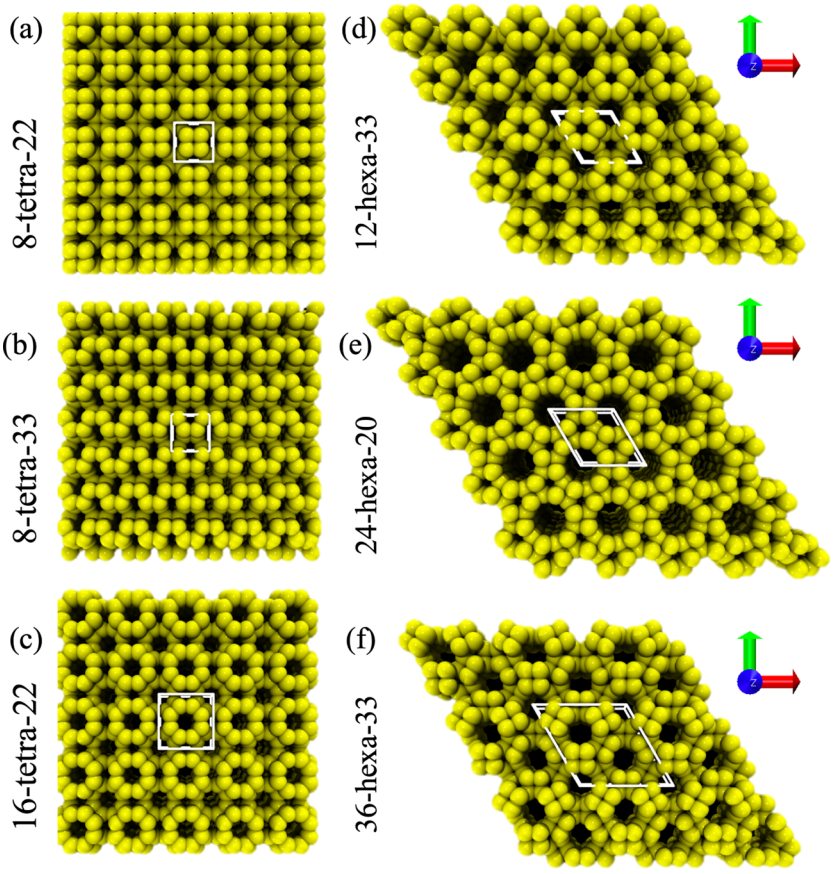

Figure 1. Schematic representation of the Tubulane structures: (a) 8-tetra-22, (b) 8-tetra-33, (c) 16-tetra-22, (d) 12-hexa-33, (e) 24-hexa-20, and (f) 36-hexa-33.

Table 1. Summary of the Calculated Structural Parameters for all Tubulane Structures

structure	atoms	tubule type of the largest channel	space group name and number	unit cell optimized lattice parameters [Å]	density [g/cm^3]
8-tetra-22	8	(2,2)	*I*4/mmm (139)	a = 4.358 b = 4.358 c = 2.497	3.425
8-tetra-33	8	(3,3)	*Imma* (74)	a = 4.922 b = 2.533 c = 4.181	3.179
16-tetra-22	16	(4,4)	*I*4/mmm (139)	a = 6.539 b = 6.539 c = 2.506	3.048
12-hexa-33	12	(3,3)	$P6_3$/mmc (194)	a = 6.090 b = 6.090 c = 2.538	2.984
24-hexa-20	24	(6,0)	*P*6/mcc (192)	a = 6.808 b = 6.808 c = 4.174	2.904
36-hexa-33	36	(3,3)	$\bar{R}3m$(166)	a = 10.451 b = 10.451 c = 2.484	3.140
diamond	8	-	$F\bar{d}3m$(227)	a = 3.579 b = 3.579 c = 3.579	3.510

RESULTS

Structural Stability

We present in Figure 1a–c the tetragonal family, with the optimized structures 8-tetra-22, 8-tetra-33, and 16-tetra-22. The unit cell is shown in white and replicated 2 × 2 × 2 times to construct the crystal. Figure 1d–f illustrates the optimized structures for the hexagonal family called supercell 12-hexa-33, 24-hexa-20, and 36-hexa-33, respectively. More detailed visualizations of the tetragonal and hexagonal structures are provided in the Supporting Information, where Figures S1 and S2 present enhanced views of the tetragonal and hexagonal families shown in Figures 1a–c and d–f, respectively, while Figures S3 and S4 display alternative orientations (axes) of the tetragonal and hexagonal structures.

Table 1 displays the structural parameters for the optimized tubulane structures calculated with CASTEP. We included the values for the cubic diamond structure for comparison. From Table 1 we observe that the diamond structure is isotropic, while the 8-tetra-33 phase is orthotropic. The other structures are transversely isotropic, exhibiting identical properties along the x and y directions but distinct behavior along the z direction. Note that 16-tetra-22 presents a density value close to that of diamond, 3.48 and 3.51 g/cm^3, respectively. The lowest density value is 2.904 g/cm^3 of the 24-hexa-20 structure.

We have also investigated the structural stability of the tubulanes at 300 K. We carried out ab initio molecular dynamics (AIMD) simulations for 2 ps in the NPT ensemble, using a time step of 1 fs. In these simulations, the unit cell of each structure was replicated 2 × 2 × 2 times. In Figures S5 and S6 in Supporting Information, we present representative AIMD snapshots for the tubulane structures, showing that tubulanes are structurally stable at room temperature (300 K). These results are significant because an approach was used to synthesize similar structures at ambient conditions.[25] Therefore, such techniques could potentially be used to create the tubulane structures.

https://doi.org/10.1021/acs.jpcc.5c08652
J. Phys. Chem. C 2026, 130, 3624−3631

Table 2. Summary of Calculated Mechanical Properties for all Tubulane Structures[a]

structure	K	$(Y_M)_x$	$(Y_M)_y$	$(Y_M)_z$	$\nu_{xy}(\nu_{yx})$	$\nu_{zx}(\nu_{xz})$	$\nu_{yz}(\nu_{zy})$
8-tetra-22	396.28	900.62	900.62	1195.35	0.172(0.172)	0.046(0.034)	0.0344(0.046)
8-tetra-33	351.94	391.17	908.17	574.04	0.113(0.263)	0.621(0.423)	−0.084(−0.053)
16-tetra-22	335.94	751.56	751.56	967.89	0.250(0.250)	0.013(0.010)	0.010(0.013)
12-hexa-33	335.20	722.71	722.71	905.14	0.227(0.227)	0.059(0.047)	0.047(0.059)
24-hexa-20	322.65	718.60	718.60	1098.43	0.198(0.198)	0.012(0.008)	0.008(0.012)
36-hexa-33	340.49	689.92	689.92	1084.43	0.271(0.271)	0.027(0.017)	0.017(0.027)
diamond	435.03	1046.31	1046.31	1046.31	0.100	0.100	0.100

[a]The Young's modulus ($(Y_M)_k$), bulk modulus (K), and Poisson's ratios (ν_{ij}) are presented, where ν_{ij} denotes the transverse strain along the j direction induced by an applied uniaxial strain along the i direction. $(Y_M)_k$ and K are given in GPa

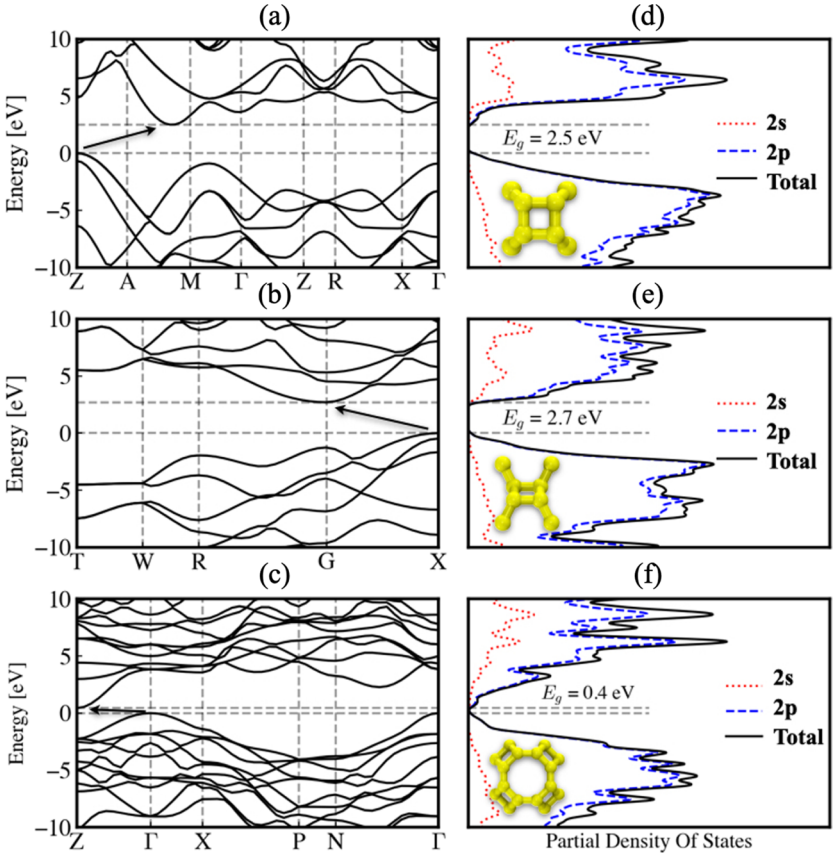

Figure 2. Electronic band structures along the high-symmetry paths of the Brillouin zone (a−c) and projected density of states (d−f) for the tetragonal Tubulane structures shown in Figure 1a−c. Panels (a,d) correspond to the 8-tetra-22 structure, panels (b,e) to the 8-tetra-33 structure, and panels (c,f) to the 16-tetra-22 structure.

Mechanical Properties

To determine the role of tubulane's unusual topologies in their mechanical behavior, we calculated the elastic constants using first-principles calculations provided by CASTEP. As discussed in the Methods section, the CASTEP Elastic Constants module provides the full 6 × 6 tensor of elastic constants, from which we can calculate the bulk modulus (B), Young Modulus (Y_M), and Poisson coefficients (ν) shown in Table 2.

The mechanical properties of the Tubulane structures exhibit significant anisotropy, unlike the isotropic nature of diamond, as shown in Table 2. The Young's modulus varies considerably depending on the direction, with some structures showing higher stiffness along the z direction than along the x or y directions. Notably, the 8-tetra-22 structure has a Young's modulus of 1195.35 GPa along the z-direction, exceeding that of diamond (1046.31 GPa). These results highlight the potential of Tubulanes for applications requiring high stiffness along specific axes. Additionally, the bulk modulus of 8-tetra-22 (396.28 GPa) approaches that of diamond (435.03 GPa), making it the stiffest among the Tubulane structures investigated here.

The results presented in Table 2 also reveal the highly anisotropic nature of Poisson's ratio in Tubulanes, in stark contrast to the uniform value of 0.1 observed in diamond. This directional dependence suggests that Tubulanes exhibit distinct deformation behaviors along different axes. Some structures exhibit extremely low Poisson's ratios (close to zero) along specific directions, such as 24-hexa-20 and 16-tetra-22, indicating minimal lateral contraction under axial compression. Furthermore, 8-tetra-33 exhibits auxetic behavior (negative Poisson's ratio) in the yz plane, a property rare in conventional materials. This auxetic property can be helpful in mechanically responsive materials that expand under tension.

https://doi.org/10.1021/acs.jpcc.5c08652
J. Phys. Chem. C 2026, 130, 3624−3631

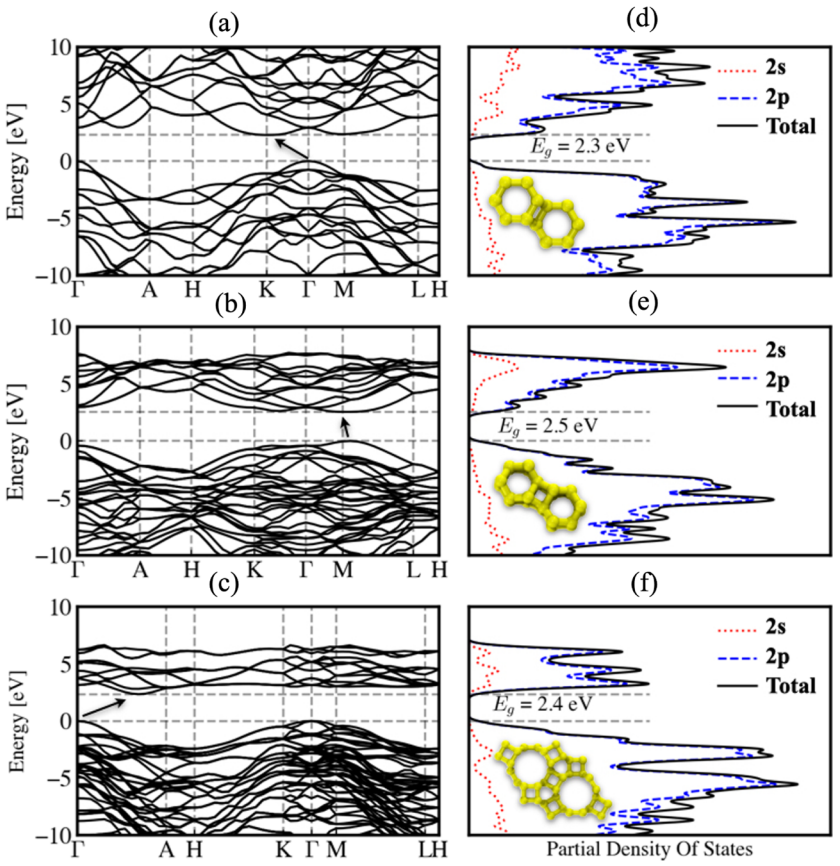

Figure 3. Electronic band structures along the high-symmetry paths of the Brillouin zone (a–c) and projected density of states (d–f) for the hexagonal Tubulane structures shown in Figure 1d–f. Panels (a,d) correspond to the 12-hexa-33 structure, panels (b,e) to the 24-hexa-20 structure, and panels (c,f) to the 36-hexa-33 structure.

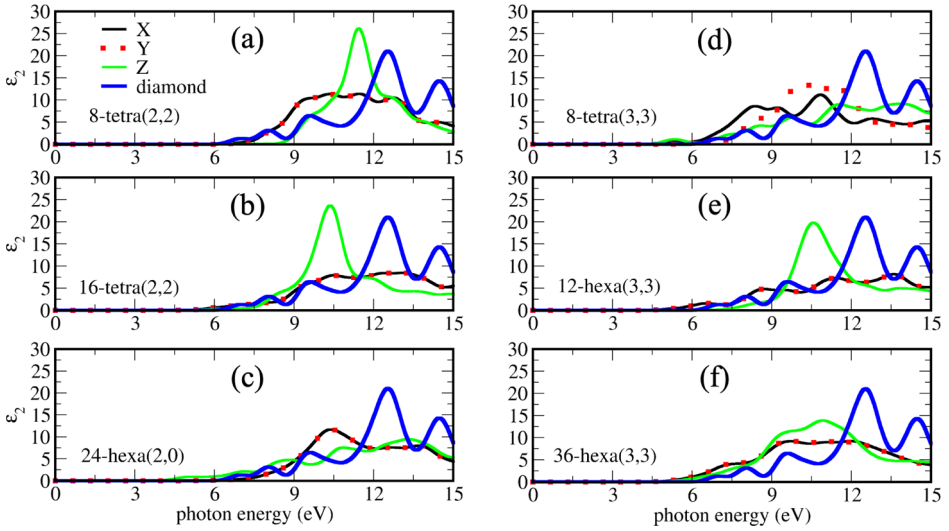

Figure 4. Imaginary part of the dielectric function versus photon energy, for an externally applied electric field polarized along the *x*, *y*, and *z* directions for all systems: 8-tetra(2,2) (a), 16-tetra(2,2) (b), 24-hexa(2,0) (c), 8-tetra(3,3) (d), 12-hexa(3,3) (e), and 36-hexa(3,3) (f).

Electronic Properties

In Figure 2, we present the calculated electronic band structure and the corresponding projected density of states (PDOS) of valence atomic orbitals 2s and 2p for the tetragonal optimized geometries shown in Figure 1a–c. The unit cell is highlighted in yellow.

We note that tetragonal structures exhibit indirect electronic band gaps of 2.5, 2.7, and 0.4 eV for 8-tetra-22, 8-tetra-33, and 16-tetra-22, respectively, consistent with the trend in direct/indirect band gaps. Intriguingly, the 8-tetra-22 and 16-tetra-22 structures differ only in the nanotube chiralities, namely (2,2) and (4,4), yet display markedly different band gap values. This behavior can be understood by considering the formation mechanism of Tubulane structures, in which carbon nanotubes

https://doi.org/10.1021/acs.jpcc.5c08652
J. Phys. Chem. C 2026, 130, 3624–3631

are subjected to high pressure until intertube bonding leads to a three-dimensional equilibrium network. Structural inspection reveals that 16-tetra-22 is the only configuration in which the tubular units remain clearly identifiable and comparatively less distorted. In contrast, the other structures undergo more pronounced deformations, as shown in Figures S1−S4 in the Supporting Information. The reduced degree of deformation in 16-tetra-22 preserves extended tubular segments with electronic characteristics closer to those of the parent metallic nanotube, maintaining a higher degree of π-orbital delocalization. In contrast, the more substantial distortions observed in the remaining Tubulane structures enhance symmetry breaking and promote π-orbital rehybridization, which are well-established mechanisms for band gap opening in strained carbon nanotubes. Consequently, the weaker structural distortion in 16-tetra-22 naturally yields a smaller band gap, whereas the more severely deformed structures exhibit larger band gaps.

We observe from the PDOS that the 2p atomic orbitals contribute most to the tetragonal tubulanes states. The 2s atomic orbitals will hybridize with the 2p orbitals to form sp^2 hybridization. However, this hybridization is minimal near the valence and conduction bands, as the 2s valence states contribute little to these regions.

In Figure 3, we present the electronic band structure and the corresponding PDOS for the hexagonal optimized geometries shown in Figure 1d−f. For the hexagonal structures, the band gap values follow the same trend as in the tetragonal case with indirect band gaps and similar values of 2.3, 2.5, and 2.4 eV for 12-hexa-33, 24-hexa-20, and 36-hexa-33, respectively. We also observe from the PDOS that hybridization occurs mainly between the 2s and 2p valence atomic orbitals.

Optical Properties

In the methodology section, we mentioned that the optical simulations were performed with the optical transition correction implemented in SIESTA, known as the SCISSOR operator. The bandgap value from Gaussian software was used to implement the correction in SIESTA.

In Figure 4, we present the imaginary part of the dielectric function as a function of the photon energy for tubulanes and diamond structures. For each structure, the first peak in the imaginary part, ϵ_2, starts for photon energy values close to the electronic bandgap values. In Table 3, we see that, except for 16-tetra-22, the structures exhibit wide band gaps. This is consistent with a high photon energy at which the imaginary part of the dielectric constant begins. Although the structure 16-tetra-22 has a small band gap, it exhibits an optical transition in the violet range. Diamond is isotropic along x, y, and z directions, as expected. In contrast, only the tubulane 8-tetra-33 is anisotropic, while the others are isotropic only along the x and y directions and anisotropic along the z direction.

Table 3. Summary of the Calculated Electronic Properties for all Tubulane Structures[a]

structure	$E_{gap,CASTEP(PBE)}$ (PBE/DFT-D)	$E_{gap,Gaussian(HSE06)}$
8-tetra-22	2.52 (2.49)	3.76
8-tetra-33	2.74 (2.70)	3.81
16-tetra-22	0.46 (0.44)	1.53
12-hexa-33	2.30 (2.28)	4.24
24-hexa-20	2.61 (2.55)	3.83
36-hexa-33	2.45 (2.35)	3.83
diamond	4.15 (4.19)	5.40

[a]All energy values are in eV.

Figure S7 shows the real part of the dielectric function as a function of photon energy. From these curves, we extracted the static dielectric constant for each structure, taking the value in the limit of high frequencies, or equivalently, for photon energy at zero. For diamond, the value is 5.4, which is in agreement with the experimental value.[26] For tubulanes, the static dielectric constant is very close to the diamond value, and the maximum difference is smaller than 0.5.

In Figure 5, we present the absorption coefficient as a function of photon energy. We observe that, for tubulanes, the trends are very similar to those of diamond, and the peak of maximum absorption intensity is very close. The absorption begins in the ultraviolet, as expected for systems with significant band gaps. For tubulanes, we observe that the absorption coefficient attains its maximum when the external electric field is polarized along the z direction.

In Figure S8 we present the refractive index as a function of photon energy for the diamond and tubulanes. The behavior of tubulanes is very similar to that of diamond, in which only the peak of maximum intensity is located at different photon energies. The refractive index for each structure is obtained when the photon energy approaches zero, corresponding to the low-frequency limit. The diamond has a refractive index of 2.33, which is close to the experimental value of 2.4.[27] For tubulanes, the values are very close to diamond, with a maximum difference of only 0.2.

In Figure 6, we have the reflectivity as a function of photon energy for tubulanes and diamond structures. The curves are very similar and exhibit their smallest values in the infrared region, increasing until they reach their maximum in the ultraviolet region. In the ultraviolet region, where absorption is maximum for photon energies near 14−15 eV, the reflectivity is also maximum, with nearly 70% of the incident light reflected. This is one indication that tubulanes can be used in ultraviolet block devices.

CONCLUSIONS

Our study highlights the unique combination of anisotropic mechanical, electronic, and optical properties exhibited by Tubulanes-cross-linked carbon nanotube structures. Unlike diamond, these materials display direction-dependent mechanical behavior, with some structures surpassing diamond's bulk and Young's modulus along specific directions. The ability to tune mechanical properties by selecting the compression direction makes them particularly attractive for applications requiring high-strength yet adaptable materials. Additionally, the anisotropic Poisson's ratio, with near-zero values in certain directions and auxetic behavior in specific cases, further expands their potential for tailored mechanical applications. From an electronic perspective, all studied Tubulanes exhibit indirect electronic band gaps, with values smaller than that of diamond.

Furthermore, the intrinsic porosity of these structures offers advantages over denser materials, such as diamond, enabling applications where a balance between mechanical resilience, lightweight properties, and permeability is required. Overall, the unique combination of high mechanical strength, tunable anisotropy, electronic versatility, and porosity positions Tubulanes-cross-linked carbon nanotube structures as promising materials for next-generation nanodevices, impact-resistant coatings, and advanced electronic applications. Their tunable nature makes them well-suited for application-specific opti-

https://doi.org/10.1021/acs.jpcc.5c08652
J. Phys. Chem. C 2026, 130, 3624−3631

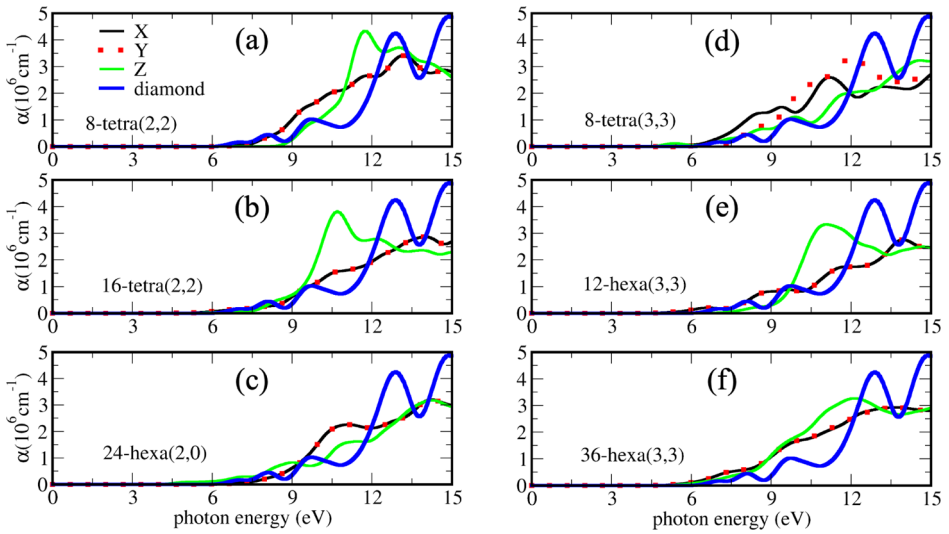

Figure 5. Absorption coefficient as a function of the photon energy, for an externally applied electric field polarized along the *x*, *y*, or *z* direction for all systems: 8-tetra(2,2) (a), 16-tetra(2,2) (b), 24-hexa(2,0) (c), 8-tetra(3,3) (d), 12-hexa(3,3) (e), and 36-hexa(3,3) (f).

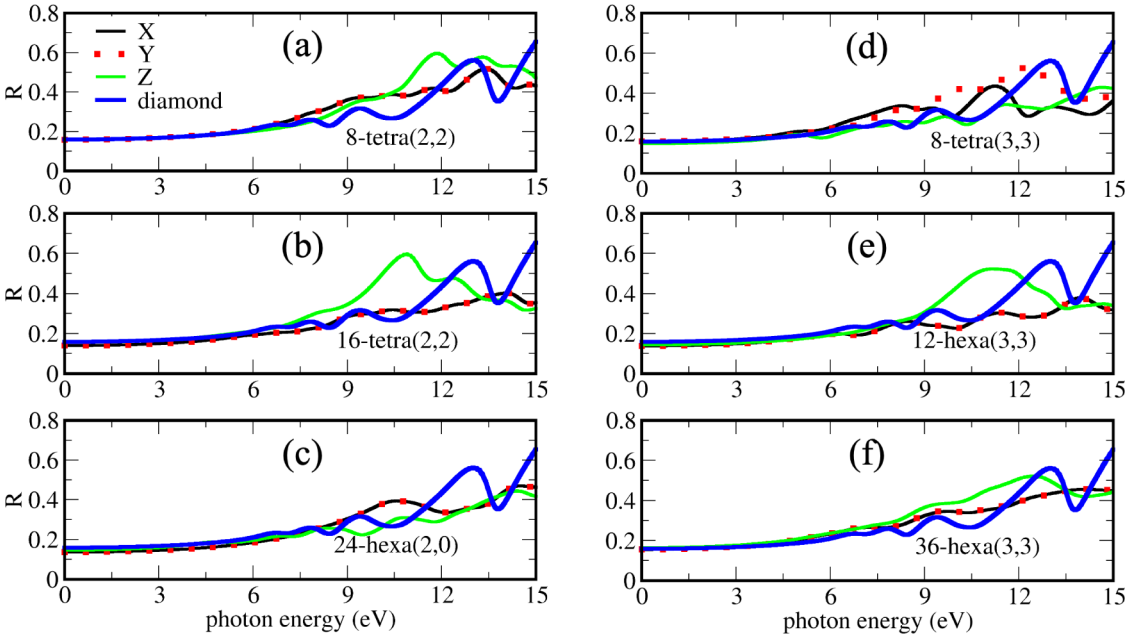

Figure 6. Reflectivity as a function of the photon energy, for an externally applied electric field polarized along the *x*, *y*, or *z* directions for all systems: 8-tetra(2,2) (a), 16-tetra(2,2) (b), 24-hexa(2,0) (c), 8-tetra(3,3) (d), 12-hexa(3,3) (e), and 36-hexa(3,3) (f).

mization, paving the way for innovative material design strategies. Given recent advances in the synthesis of 3D carbon-based carbons, the synthesis of tubulane-like structures is within current technological capabilities.

■ ASSOCIATED CONTENT

Supporting Information

The Supporting Information is available free of charge at https://pubs.acs.org/doi/10.1021/acs.jpcc.5c08652.

CIF details for 8-tetra-22, 8-tetra-33, 16-tetra-22, 12-hexa-33, 24-hexa-20, and 36-hexa-33 (ZIP)

Detailed structural views of tetragonal and hexagonal tubulanes, alternative axis orientations (Figures S1 and S2), supercell representations (Figures S3 and S4), AIMD snapshots at 300 K (Figures S5 and S6), and complementary optical properties including the real dielectric function and refractive index spectra (Figures S7 and S8) (PDF)

■ AUTHOR INFORMATION

Corresponding Authors

Marcelo L. Pereira Junior − *Department of Electrical Engineering, College of Technology, University of Brasília, Brasília, Distrito Federal 70910-900, Brazil; Department of Materials Science and NanoEngineering, Rice University, Houston, Texas 77005, United States;* orcid.org/0000-0001-9058-510X; Email: marcelo.lopes@unb.br

Douglas S. Galvao − *Department of Applied Physics and Center for Computational Engineering and Sciences, University of Campinas, Campinas, São Paulo 13083-970, Brazil;*

https://doi.org/10.1021/acs.jpcc.5c08652
J. Phys. Chem. C 2026, 130, 3624−3631

orcid.org/0000-0003-0145-8358; Email: galvao@ifi.unicamp.br

Authors

Raphael M. Tromer − *Institute of Physics, University of Brasília, Brasília, Distrito Federal 70910-900, Brazil*

Bruno Ipaves − *Department of Applied Physics and Center for Computational Engineering and Sciences, University of Campinas, Campinas, São Paulo 13083-970, Brazil;* orcid.org/0000-0003-2908-4589

Cristiano F. Woellner − *Department of Physics, Federal University of Paraná, Curitiba, Paraná 81531-980, Brazil; Interdisciplinary Center for Science, Technology, and Innovation (CICTI), Federal University of Paraná, Curitiba, Paraná 81530-000, Brazil*

Kun Cai − *School of Science, Harbin Institute of Technology, Shenzhen 518055, China*

Complete contact information is available at: https://pubs.acs.org/10.1021/acs.jpcc.5c08652

Funding

The Article Processing Charge for the publication of this research was funded by the Coordenacao de Aperfeicoamento de Pessoal de Nivel Superior (CAPES), Brazil (ROR identifier: 00x0ma614).

Notes

The authors declare no competing financial interest.

■ ACKNOWLEDGMENTS

In memory of Professor Ray H. Baughman, to whom the authors dedicate this work, in recognition of his inspiring scientific contributions and lasting influence. This work was partially financed by the Coordination for the Improvement of Higher Education Personnel (CAPES), the Brazilian National Council for Scientific and Technological Development (CNPq), and the São Paulo Research Foundation (FAPESP). The authors thank the Center for Computational Engineering & Sciences (CCES) at Unicamp for financial support through the FAPESP/CEPID Grant 2013/08293-7. B.I. acknowledges financial support from CNPq (process number #153733/2024-1) and FAPESP (process number #2024/11016-0). M.L.P.J. acknowledges financial support from the Federal District Research Support Foundation (FAPDF, grant 00193-00001807/2023-16), CNPq (grants 444921/2024-9 and 308222/2025-3), and CAPES (grant 88887.005164/2024-00). D.S.G. also acknowledges INEO/CNPq and FAPESP grant 2025/27044-5.

■ REFERENCES

(1) Baughman, R.; Galvao, D. Tubulanes: carbon phases based on cross-linked fullerene tubules. *Chem. Phys. Lett.* **1993**, *211*, 110−118.
(2) Rysaeva, L. K.; Baimova, J. A.; Dmitriev, S. V.; Lisovenko, D. S.; Gorodtsov, V. A.; Rudskoy, A. I. Elastic properties of diamond-like phases based on carbon nanotubes. *Diamond Relat. Mater.* **2019**, *97*, 107411.
(3) Sajadi, S. M.; Woellner, C. F.; Ramesh, P.; Eichmann, S. L.; Sun, Q.; Boul, P. J.; Thaemlitz, C. J.; Rahman, M. M.; Baughman, R. H.; Galvão, D. S.; Tiwary, C. S.; Ajayan, P. M. 3D Printed Tubulanes as Lightweight Hypervelocity Impact Resistant Structures. *Small* **2019**, *15*, 1904747.
(4) Ajayan, P.; Lijima, S. Smallest carbon nanotube. *Nature* **1992**, *358*, 23.
(5) Ebbesen, T. W.; Ajayan, P. M. Large-scale synthesis of carbon nanotubes. *Nature* **1992**, *358*, 220−222.
(6) Iijima, S. Helical microtubules of graphitic carbon. *Nature* **1991**, *354*, 56−58.
(7) Tromer, R. M.; Felix, L. C.; Woellner, C. F.; Galvao, D. S. A DFT investigation of the electronic, optical, and thermoelectric properties of pentadiamond. *Chem. Phys. Lett.* **2021**, *763*, 138210.
(8) Ipaves, B.; Justo, J. F.; Sanyal, B.; Assali, L. V. Tuning the Electronic and Mechanical Properties of Two-Dimensional Diamond through N and B Doping. *ACS Appl. Electron. Mater.* **2024**, *6*, 386−393.
(9) Pela, R. R.; Hsiao, C.-L.; Hultman, L.; Birch, J.; Gueorguiev, G. K. Electronic and optical properties of core−shell InAlN nanorods: a comparative study via LDA, LDA-1/2, mBJ, HSE06, G 0 W 0 and BSE methods. *Phys. Chem. Chem. Phys.* **2024**, *26*, 7504−7514.
(10) Filho, M. A. M.; Farmer, W.; Hsiao, C.-L.; Dos Santos, R. B.; Hultman, L.; Birch, J.; Ankit, K.; Gueorguiev, G. K. Density functional theory-fed phase field model for semiconductor nanostructures: The case of self-induced core−shell InAlN nanorods. *Cryst. Growth Des.* **2024**, *24*, 4717−4727.
(11) Mukherjee, R.; Chakrabarti, T.; Anumol, E. A.; Abinandanan, T. A.; Ravishankar, N. Thermal Stability of Spherical Nanoporous Aggregates and Formation of Hollow Structures by Sintering? A Phase-Field Study. *ACS Nano* **2011**, *5*, 2700−2706.
(12) Baughman, R. H.; Zakhidov, A. A.; De Heer, W. A. Carbon nanotubes−the route toward applications. *science* **2002**, *297*, 787−792.
(13) Clark, S. J.; Segall, M. D.; Pickard, C. J.; Hasnip, P. J.; Probert, M. I. J.; Refson, K.; Payne, M. C. First principles methods using CASTEP. *Z. Kristallogr.* **2005**, *220*, 567−570.
(14) Soler, J. M.; Artacho, E.; Gale, J. D.; García, A.; Junquera, J.; Ordejón, P.; Sánchez-Portal, D. The SIESTA method for ab initio order-N materials simulation. *J. Phys.: Condens. Matter* **2002**, *14*, 2745.
(15) Perdew, J. P.; Burke, K.; Ernzerhof, M. Generalized gradient approximation made simple. *Phys. Rev. Lett.* **1996**, *77*, 3865.
(16) Tkatchenko, A.; Scheffler, M. Accurate Molecular Van Der Waals Interactions from Ground-State Electron Density and Free-Atom Reference Data. *Phys. Rev. Lett.* **2009**, *102*, 073005.
(17) Lin, J. S.; Qteish, A.; Payne, M. C.; Heine, V. Optimized and transferable nonlocal separable ab initio pseudopotentials. *Phys. Rev. B* **1993**, *47*, 4174−4180.
(18) Monkhorst, H. J.; Pack, J. D. Special points for Brillouin-zone integrations. *Phys. Rev. B:* **1976**, *13*, 5188.
(19) Pfrommer, B. G.; Cote, M.; Louie, S. G.; Cohen, M. L. Relaxation of crystals with the quasi-Newton method. *J. Comput. Phys.* **1997**, *131*, 233−240.
(20) Fadaie, M.; Shahtahmassebi, N.; Roknabad, M. R. Effect of external electric field on the electronic structure and optical properties of stanene. *Opt. Quantum Electron.* **2016**, *48*, 440.
(21) Johnson, K. A.; Ashcroft, N. W. Corrections to density-functional theory band gaps. *Phys. Rev. B* **1998**, *58*, 15548−15556.
(22) Kishore, M. A.; Ravindran, P. Enhanced Photocatalytic Water Splitting in a C2N Monolayer by C-Site Isoelectronic Substitution. *ChemPhysChem* **2017**, *18*, 1526−1532.
(23) Nayebi, P.; Emami-Razavi, M.; Zaminpayma, E. Study of electronic and optical properties of CuInSe2 nanowires. *J. Phys. Chem. C* **2016**, *120*, 4589−4595.
(24) Ljungberg, M. P.; Vänskä, O.; Koval, P.; Koch, S. W.; Kira, M.; Sánchez-Portal, D. Charge-transfer states and optical transitions at the pentacene-TiO2 interface. *New J. Phys.* **2017**, *19*, 033019.
(25) Zhong, Y.; Cheng, B.; Park, C.; Ray, A.; Brown, S.; Mujid, F.; Lee, J.-U.; Zhou, H.; Suh, J.; Lee, K.-H.; Mannix, A. J.; Kang, K.; Sibener, S. J.; Muller, D. A.; Park, J. Wafer-scale synthesis of monolayer two-dimensional porphyrin polymers for hybrid superlattices. *Science* **2019**, *366*, 1379−1384.
(26) Batsanov, S. S.; Gavrilkin, S. M.; Batsanov, A. S.; Poyarkov, K. B.; Kulakova, I. I.; Johnson, D. W.; Mendis, B. G. Giant dielectric permittivity of detonation-produced nanodiamond is caused by water. *J. Mater. Chem.* **2012**, *22*, 11166−11172.
(27) Walker, W. C.; Osantowski, J. Ultraviolet Optical Properties of Diamond. *Phys. Rev.* **1964**, *134*, A153−A157.